Energy Dissipation Analysis for Inelastic Reinforced Concrete and Steel Beam-Columns

Han Yang[a], Yuan Feng[a], Hexiang Wang[a], Boris Jeremić[a,b,*]

[a] *Department of Civil and Environmental Engineering, University of California, Davis, CA, USA*
[b] *Earth Science Division, Lawrence Berkeley National Laboratory, Berkeley, CA, USA*

Abstract

Presented is a thermodynamics based methodology for computing energy dissipation in inelastic beam-column elements. Theoretical formulation for energy storage and dissipation in uniaxial steel fiber and concrete fiber models is derived from the principles of thermodynamics, in conjunction with a few assumptions on energy transformation and dissipation. Proposed methodology is implemented in MS-ESSI Simulator and illustrated through a number of numerical examples on beam-columns and frame models under various loading conditions. It is shown that the consideration of plastic free energy in addition to plastic work, is necessary to correctly evaluate energy dissipation in nonlinear beam-column elements. Results of energy analysis indicates that the difference between plastic work and plastic dissipation could be significant, and that the ratio between them evolves with time.

Keywords: Energy dissipation, Inelastic beam column

*Corresponding authors
Email address: `jeremic@ucdavis.edu` (Boris Jeremić)

1. Introduction

Mechanical energy in soil structure interaction (SSI) systems is dissipated during the irreversible dissipative process of energy transformation in which entropy of the system increases. Energy dissipation has been used, directly or indirectly, as a key parameter to evaluate damage in elastic-plastic materials. A common misconception about plastic work and energy dissipation due to plasticity has been noticed in a number of recent publications [45, 23, 42, 39, 43, 48, 30] in which violations of the second law of thermodynamics is observed. As presented in an earlier paper [49], the correct formulation for energy analysis on elastic-plastic solids has been derived from the second law of thermodynamics. The theoretical and computational framework has been verified through system energy balance in a series of numerical studies on elastic and elastic-plastic material models. The purpose of this paper is to present a methodology for correctly evaluating energy dissipation in nonlinear fiber beam-column structural elements.

Early work reported by Farren and Taylor [12] and Taylor and Quinney [44] showed that plastic free energy could be significant in metals, thus should not be neglected without reasoning. The ratio of plastic work converted into heat, usually referred to as the Quinney–Taylor coefficient, was measured to be between 0.6 to 1.0 [1, 52, 11, 33]. Mason et al. [26] pointed out that the Quinney–Taylor coefficient is both strain and strain rate dependent but could be assumed to be a constant in most cases. A constitutive model for metals was presented by Rosakis et al. [36], Hodowany et al. [16], Ravichandran et al. [35] based on thermoplasticity. Presented model can model the evolution of energy dissipation and has been validated through experiments. Semnani et al. [38] presented a thermoplastic framework that could predict strain localization in transversely isotropic materials.

Despite of the existence of sophisticated theories that are capable of modeling the evolution of energy dissipation, including those mentioned earlier, most constitutive relationships used to model structural elements do not involve thermodynamics or thermoplasticity. One commonly used finite element (FE) technique to model inelastic frame structures, is to use nonlinear beam-column finite element, and nonlinear fiber sections. In this approach, a beam-column element is analyzed using a number of cross sections, at locations of integration points. Such cross sections are divided into a number of uniaxial fibers with various constitutive models, for steel and/or concrete for example. This model have been proved to be able to capture nonlinear stress–strain behaviors of structural elements under axial loading and/or pure bending.

Problems arise when such elements are used to calculate energy dissipation. As observed in many publications [21, 53, 15, 46, 51, 32], energy dissipation analysis was performed using hysteretic stress–strain and/or force–displacement response of the elements. Hysteretic stress–strain and/or force–displacement responses corresponds to plastic work. Plastic work is not the same as plastic energy dissipation. It is also important to point out that various damage indices that are used to evaluate seismic performance of frame structures are derived from energy dissipation. It is then noted that such damage indices are not valid if the fundamental computation of energy dissipation is incorrect.

It has been shown by Dafalias et al. [8], Feigenbaum and Dafalias [13], Yang et al. [49] that the difference between plastic work and plastic dissipation is the plastic free energy, or cold work, which can be calculated from material internal variables (or state variables). This computation can be performed on solids modeled with elastic-plastic constitutive relations in which internal variables are updated at every increment. On the other hand, constitutive relationships used to model nonlinear structural elements based on fiber cross section are mainly based on empirical fitting of experimental results [40, 41, 22, 34, 25, 3, 47, 20]. The parameters used in these models are different than internal variables that are used in elastic-plastic constitutive models for solids. In order to apply rational mechanics for computing energy dissipation, a new methodology is needed. This new methodology, based on thermodynamics, should be able to correctly evaluate energy storage and dissipation in structural elements, while using the same fiber material models for steel and concrete.

During the recent few decades, a number of studies have been conducted with focus on energy analysis of SSI systems [45, 23, 18, 43, 15, 29, 28, 10]. Despite different formulations used, the calculations of energy dissipation due to hysteretic damping (material elasto-plasticity) in these publications were all performed without consideration of plastic free energy, which leads to the violation of the second principle of thermodynamics. In other words, results show negative incremental energy dissipation, which is equivalent to energy production. It is worth pointing out that such problem can be found in many other publications in the last few decades.

In order to correctly evaluate energy dissipation in nonlinear beam-column elements modeled using fiber sections, the thermo-mechanics framework must be applied to the uniaxial constitutive models used for fibers. Focus of this paper is on proper modeling of different forms of energy storage and dissipation in uniaxial material models. Presented is a theoretical and computational formulations for computing energy dissipation in uniaxial concrete and steel fiber models. A series of FE simulations are carried out using the MS-ESSI Simulator [17] to illustrate the energy behavior of structural frame systems. The method is verified by comparing the input work and the energy storage and dissipation in the system. The difference between accumulated plastic work and accumulated plastic dissipation, which can be significant in many cases, is addressed. Finally, conclusions on plastic energy dissipation in structural elements are drawn from the verified results.

2. Theoretical and Computational Formulations

2.1. Thermomechanical Framework

The theory of continuum thermo-mechanics has been discussed in a number of earlier publications by Lubliner [24] and Rosakis et al. [36], from which the fundamental framework of this study is derived. General equations of elastoplasticity and thermodynamics are modified using few plausible assumptions to accommodate use of existing fiber material models. Small deformation theory is assumed, so that the small strain tensor ϵ_{ij} is used to describe deformation of a material. It is noted that all equations in this paper are expressed in index notation.

The general thermomechanical process is governed by momentum balance and the first and second law of thermodynamics. The localized version of the first law of thermodynamics (energy balance equation) is given in the form:

$$\sigma_{ij}\dot{\epsilon}_{ij} + q_{i,i} + \rho r = \rho \dot{e} \tag{1}$$

where σ_{ij} is Cauchy stress, the term $\sigma_{ij}\epsilon_{ij}$ is called the stress power, q_i are the components of the heat flux vector, ρ is the mass density of the material, r is the heat supply per unit volume, and e is the internal energy per unit volume. Standard definition of stress from mechanics of materials, i.e. positive in tension, is used.

The localized version of the second law of thermodynamics (Clausius–Duhem inequality) is expressed as:

$$\rho\dot{\eta} - (\frac{q_i}{\theta})_{,i} - \frac{1}{\theta}\rho r \geq 0 \tag{2}$$

where η is the entropy per unit volume and θ is the absolute temperature.

Substituting the heat supply per unit volume r in Equation 2 with the expression from Equation 1, and introducing the rate of change of internal dissipation per unit volume Φ gives:

$$\rho\theta\dot{\eta} - \rho\dot{e} + \sigma_{ij}\dot{\epsilon}_{ij} + \frac{1}{\theta}q_i\theta_{,i} = \Phi + \frac{1}{\theta}q_i\theta_{,i} \geq 0 \tag{3}$$

Note that the internal dissipation can have many sources, including material plasticity, viscous coupling, and other forms of energy dissipation.

The Helmholtz free energy per unit volume ψ, which is referred to as free energy in this paper, is defined as:

$$\psi = e - \theta\eta \tag{4}$$

The second law of thermodynamics can be expressed in terms of free energy ψ as:

$$\Phi + \frac{1}{\theta}q_i\theta_{,i} = -\rho\dot{\psi} - \rho\dot{\theta}\eta + \sigma_{ij}\dot{\epsilon}_{ij} + \frac{1}{\theta}q_i\theta_{,i} \geq 0 \tag{5}$$

The rate of internal dissipation per unit volume Φ can be written as:

$$\Phi = \sigma_{ij}\dot{\epsilon}_{ij} - \rho\dot{\psi} - \rho\dot{\theta}\eta \tag{6}$$

At this point, a few assumptions are introduced to simplify the governing equations. According to Feigenbaum and Dafalias [13], Collins and Houlsby [6], Collins [4], Collins and Kelly [5], it can be assumed that the deformation of beam-column elements under earthquake loading is approximately isothermal, which indicates that the temperature field θ is constant and uniform.

This approximation is reasonable considering the fact that seismic energy is mostly carried by the low-frequency components of earthquake ground motion, which allows the heat generated in the material to be largely dissipated. With this assumption, the rate of internal dissipation Φ is simplified into the form:

$$\Phi = \sigma_{ij}\dot{\epsilon}_{ij} - \rho\dot{\psi} \geq 0 \tag{7}$$

Next, all material models studied in this paper are assumed to be decoupled, which means that the (small) strain tensor can be additively decomposed into elastic and plastic parts:

$$\epsilon_{ij} = \epsilon_{ij}^{el} + \epsilon_{ij}^{pl} \tag{8}$$

Lubliner [24] and Collins and Houlsby [6] showed that this assumption can be deduced if the instantaneous elastic moduli of a material are independent of the internal variables. Under the assumption of decoupled material, the free energy ψ can also be decomposed into elastic and plastic parts:

$$\psi = \psi_{el} + \psi_{pl} \tag{9}$$

where the elastic part of the free energy ψ_{el} is also known as the elastic strain energy. Elastic strain energy is defined in incremental form as:

$$\dot{\psi}_{el} = \sigma_{ij}\dot{\epsilon}_{ij}^{el} \tag{10}$$

By substituting Equation 8, Equation 9, and Equation 10 into Equation 7, the rate of internal dissipation Φ can be expressed in terms of the rate of plastic free energy $\dot{\psi}_{pl}$:

$$\Phi = \sigma_{ij}\dot{\epsilon}_{ij} - \sigma_{ij}\dot{\epsilon}_{ij}^{el} - \rho\dot{\psi}_{pl} \geq 0 \tag{11}$$

Equation 11 represents two basic principles that should always be upheld in any energy analysis for decoupled material undergoing isothermal process:

- The stress power that is input into a material body by external loading is transformed into elastic strain energy, plastic free energy, and material internal dissipation. All forms of energy must be considered to maintain energy balance of the material body. This principle ensures that the first law of thermodynamics holds.

- The rate of change of material internal dissipation (plastic dissipation) is nonnegative at any time. In other words, accumulated internal dissipation can not decrease during any time period. This principle ensures that the second law of thermodynamics holds.

2.2. Plastic Free Energy

The physical nature of plastic free energy is associated with the material micro-structure. For particulate materials, plastic free energy will be accumulated or released if there is evolution of particle arrangement (micro-fabric). Evolution of particle arrangement happens as soon as the material is loaded. For other materials, for example metals, micro-structures is represented by the shape and arrangement of the crystals, whose evolution will result in change in plastic free energy. Detailed explanations of the evolution of plastic free energy can be found in publications by Besseling and Van Der Giessen [2], Collins and Kelly [5], and Yang et al. [49].

Using Equation 11, the energy dissipation of any elastic-plastic material under isothermal loading process can be calculated, provided that all the terms on the right hand side of the equation are known. For most elastic-plastic constitutive models, the stress tensor σ_{ij} and the elastic strain tensor ϵ_{ij}^{el} are being calculated as simulation progresses. The challenging task is to evaluate the plastic free energy term ψ_{pl}, whose formulation depends on the internal variables used in the constitutive model.

For a decoupled elastic-plastic material model that exhibits both isotropic and kinematic hardening, the plastic free energy is decomposed into isotropic and kinematic parts, that are calculated separately and then summed up. The formulation of plastic free energy for this type of material was given by Feigenbaum and Dafalias [13]:

$$\psi_{pl} = \psi_{pl}^{iso} + \psi_{pl}^{kin} = \frac{1}{2\rho\kappa_1}k^2 + \frac{1}{2\rho a_1}\alpha_{ij}\alpha_{ij} \tag{12}$$

where ψ_{pl}^{iso} and ψ_{pl}^{kin} are the isotropic and kinematic parts of the plastic free energy, respectively, k is the radius of yield surface, α is the back stress, κ_1 and a_1 are non-negative material constants. Note that Equation 12 can be used for a wide range of constitutive models with various yield functions, including von Mises and Drucker-Prager yield criteria whose energy behavior has been studied and presented by Yang et al. [49]. Such materials are usually used to model solids (soil and mass concrete).

On the other hand, frame structures are usually modeled using beam-column elements in combination with fiber sections and uniaxial material models. In this case, Equation 12 does not apply. It is noted that most uniaxial constitutive models that are used for concrete and steel modeling [27, 14, 50], were not developed with thermodynamics based energy dissipation in mind. Therefore, material model definitions for concrete and steel were appraised using thermodynamics framework [49] in order to correctly evaluate energy storage and dissipation in these materials.

2.3. Energy Dissipation in Beam-Column Element

Beams and columns are modeled with nonlinear, displacement-based beam-column element, that is available within the MS-ESSI Simulator. In order to incorporate confined/unconfined concrete and steel reinforcement in beam-column element, fiber sections are assigned with corresponding material model uniaxial fibers. An example model is shown in Figure 1. Model

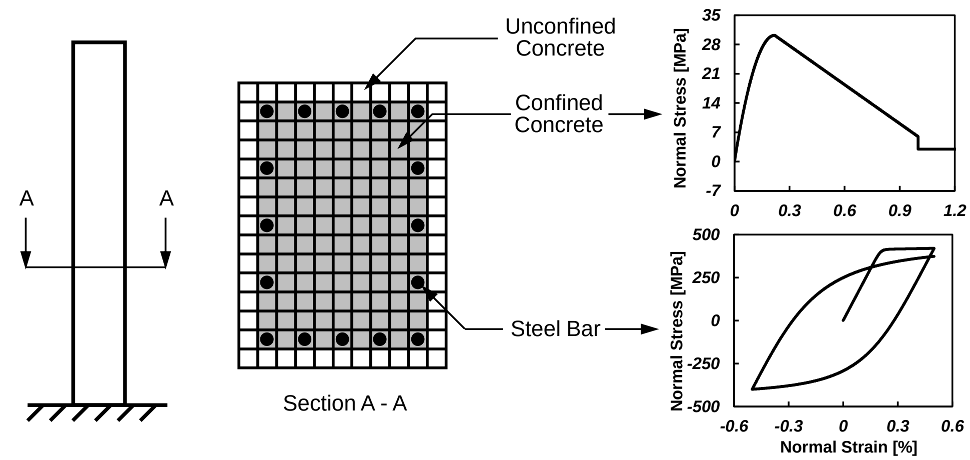

Figure 1: Schematic of a bottom-fixed column modeled with concrete and steel fibers.

represents a bottom-fixed, cantilever reinforced concrete column Figure 1 also shows constant beam-column cross section, as well as constitutive response of concrete and steel fibers. This model is analyzed later, it is presented here in order to illustrate nonlinear model for a beam-column element with fiber cross section, and individual fiber constitutive response.

2.3.1. Uniaxial Steel Fiber

The uniaxial steel material model examined in this study was developed by Menegotto and Pinto [27] and extended by Filippou et al. [14]. This uniaxial steel model is capable of capturing the nonlinear hysteretic behavior and isotropic strain-hardening effect of steel. The uniaxial stress–strain response of steel material is shown in Figure 2, along with explanation of material parameters. The model, as presented by Menegotto and Pinto [27],

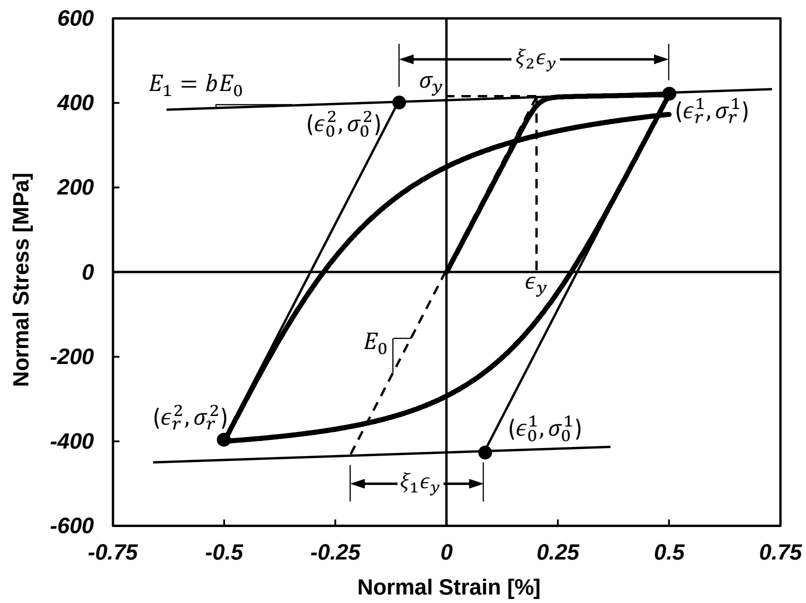

Figure 2: Constitutive model for uniaxial steel fiber (after Menegotto and Pinto [27]).

takes on the form:

$$\sigma^* = b\epsilon^* + \frac{(1-b)\epsilon^*}{(1+\epsilon^{*R})^{1/R}} \tag{13}$$

with

$$\epsilon^* = \frac{\epsilon - \epsilon_r}{\epsilon_0 - \epsilon_r}; \quad \sigma^* = \frac{\sigma - \sigma_r}{\sigma_0 - \sigma_r} \tag{14}$$

where b is the strain-hardening ratio, ϵ_r and σ_r are the strain and stress at the point of strain reversal, ϵ_0 and σ_0 are the strain and stress at the point of intersection of the two asymptotes, R is the curvature parameter that governs the shape of the transition curve between the two asymptotes. Note that this model is defined for uniaxial material, in which the stresses and strains are scalars instead of tensors. Therefore, beam-column finite element that uses this model for section modeling is defined for pure bending and pure compression, tension.

The expression for the curvature parameter R is suggested by Menegotto and Pinto [27]:

$$R = R_0 - \frac{c_{R_1}\xi}{c_{R_2} + \xi} \tag{15}$$

where R_0 is the value of the curvature parameter R during initial loading, c_{R_1} and c_{R_2} are degradation parameters that need to be experimentally determined. The parameter ξ, that is updated after strain reversal, is defined as:

$$\xi = \left| \frac{(\epsilon_m - \epsilon_0)}{\epsilon_y} \right| \tag{16}$$

where ϵ_m is the maximum (or minimum) strain at the previous strain reversal point, depending on the loading direction of the material. If the current incremental strain is positive, the parameter ϵ_m takes the value of the maximum reversal strain. Parameter ϵ_y is the monotonic yield strain.

In order to capture isotropic hardening behavior, Filippou et al. [14] introduced stress shift mechanism into the original model by Menegotto and Pinto [27]. Note that the hardening rate in compression and tension can be different by choosing different hardening parameters for compression and tension. The proposed relation takes the form:

$$\frac{\sigma_{st}}{\sigma_y} = a_1 \left(\frac{\epsilon_{max}}{\epsilon_y} - a_2 \right) \tag{17}$$

where σ_{st} is the shift stress that determines the shift of yield asymptote, ϵ_{max} is the absolute maximum strain at strain reversal, and a_1 and a_2 are hardening parameters in compression that are experimentally determined. In the case of tension, the hardening parameters a_1 and a_2 in Equation 17 are replaced by a_3 and a_4, respectively. Parameters a_3 and a_4 are also determined by experiment.

The energy computation procedure for this uniaxial steel model is shown in Figure 3, and it follows the thermomechanical framework established earlier in this paper.

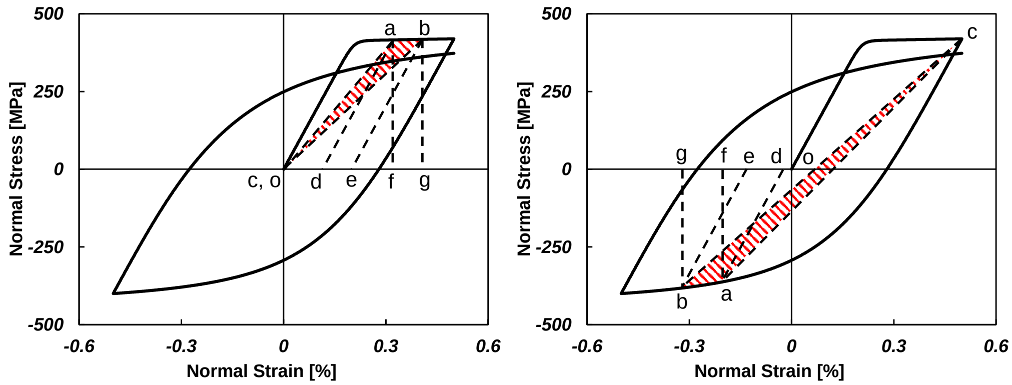

(a) (b)

Figure 3: Energy computation of uniaxial steel fiber: (a) Monotonic loading branch; (b) Cyclic loading branch.

Note that the only difference between the monotonic loading branch (Figure 3(a)) and the cyclic loading branch (Figure 3(b)) is that the strain reversal point c is at the origin o in the monotonic case. The following explanation of the proposed energy computation method applies to both monotonic and cyclic loading scenarios.

Firstly, the elastic strain energy density E_S is defined in accordance with the classic assumption that it is only a function of current stress state of the material:

$$E_S = E_S(\sigma) = \frac{1}{2E_0}\sigma^2 \tag{18}$$

Graphically, the elastic strain energy density of the material shown in Figure 3 at states a and b are the triangular areas afd and bge, respectively. Then the incremental form of Equation 18 is simply:

$$dE_S = \frac{1}{E_0}\sigma d\sigma \tag{19}$$

Next, the incremental plastic dissipation density D_P from state a to state

b is assumed to be the triangular area abc:

$$dD_P = \frac{1}{2}[(\sigma - \sigma_r)d\epsilon - (\epsilon - \epsilon_r)d\sigma] \tag{20}$$

This assumption ensures that the incremental plastic dissipation is non-negative, satisfying one of the two basic principles of thermodynamics.

One special case to consider is when the material exhibits no cyclic softening, in other words, material micro-structure is not evolving. In this case a perfectly overlapping stress–strain loops will be observed. In this case only, the energy dissipation calculated using Equation 20 for one cyclic will be represented by the area of the hysteresis loop. In thermodynamics, the area of hysteresis loop is equal to the plastic work, rather than plastic dissipation, however in the case of non-evolving material structure, plastic work becomes equal to plastic dissipation. It is important to stress that this is true only in this case.

For a general case, where the material does exhibit cyclic softening, plastic free energy density E_P is graphically represented by the areas of polygon $adoca$ and polygon $beocb$ at states a and b, respectively. The plastic free energy calculated using this assumption is given by:

$$E_P = \frac{1}{2}\left[\sigma\left(\epsilon - \frac{\sigma}{E_0} - \epsilon_r\right) + \sigma_r\epsilon\right] \tag{21}$$

The incremental form of Equation 21 is given as:

$$dE_P = \frac{1}{2}\left[(\sigma + \sigma_r)\,d\epsilon + \left(\epsilon - \frac{1}{E_0}\sigma - \epsilon_r\right)d\sigma\right] \tag{22}$$

Adding Equations 19, 20, and 22, the incremental form of energy balance is written as:

$$dE_S + dE_P + dD_P = \sigma d\epsilon \tag{23}$$

where the increment of three energy components add up to the increment of stress power during any loading step.

2.3.2. Uniaxial Concrete Fiber

The uniaxial concrete material model used in this study is based on the model proposed by Yassin [50]. This model is capable of modeling the nonlinear hysteretic behavior and damage effects in concrete. The material parameters and stress–strain response of this material are shown in Figure 4.

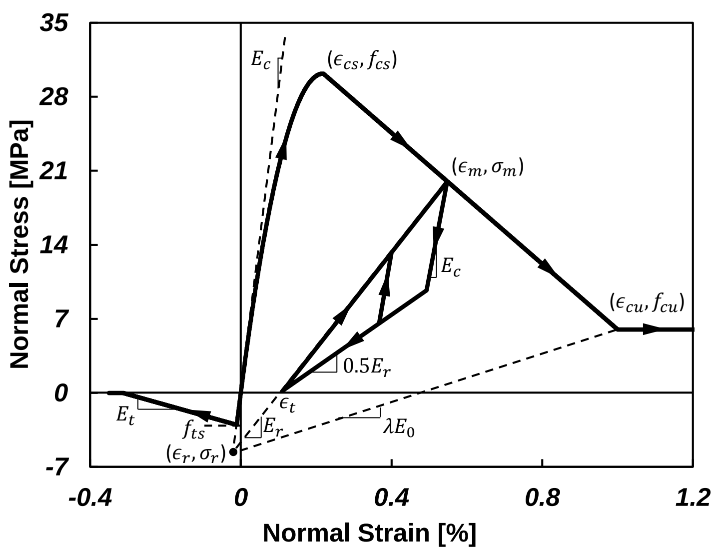

Figure 4: Constitutive model for uniaxial concrete fiber (after Yassin [50]).

The monotonic envelope curve of this model in compression is based on the model of Kent and Park [19] and later generalized by Scott et al. [37]. For a given strain ϵ_c, the compressive stress σ_c and corresponding tangent stiffness E are given as:

$$\epsilon_c \leq \epsilon_{cs} \quad ; \quad \sigma_c = f_{cs}\left[2\left(\frac{\epsilon_c}{\epsilon_{cs}}\right) - \left(\frac{\epsilon_c}{\epsilon_{cs}}\right)^2\right] \quad ; \quad E = E_c\left(1 - \frac{\epsilon_c}{\epsilon_{cs}}\right) \tag{24}$$

$$\epsilon_{cs} < \epsilon_c \leq \epsilon_{cu} \quad ; \quad \sigma_c = \frac{\epsilon_c - \epsilon_{cs}}{\epsilon_{cu} - \epsilon_{cs}}(f_{cu} - f_{cs}) + f_{cs} \quad ; \quad E = \frac{f_{cu} - f_{cs}}{\epsilon_{cu} - \epsilon_{cs}} \tag{25}$$

$$\epsilon_c > \epsilon_{cu} \quad ; \quad \sigma_c = f_{cu} \quad ; \quad E = 0 \tag{26}$$

where f_{cs} is the maximum compressive strength of the concrete material, ϵ_{cs} is the concrete strain at compressive strength, f_{cu} is the ultimate (crushing) strength of the concrete material, ϵ_{cu} is the concrete strain at ultimate strength, and E_c is the initial concrete tangent stiffness that can be calculated using the equation:

$$E_c = \frac{2f_{cs}}{\epsilon_{cs}} \tag{27}$$

All material parameters should be determined experimentally.

The cyclic behavior of concrete model in compression is shown in Figure 4. One assumption of this model is that all reloading lines intersect at a common point, where the stress σ_r and strain ϵ_r are given by the following expressions:

$$\epsilon_r = \frac{f_{cu} - \lambda E_c \epsilon_{cu}}{E_c(1-\lambda)} \tag{28}$$

$$\sigma_r = E_c \epsilon_r \tag{29}$$

After unloading from a point on the compressive monotonic envelope, the model response is bounded by two lines that are defined by:

$$\sigma_{max} = \sigma_m + E_r(\epsilon_c - \epsilon_m) \tag{30}$$

$$\sigma_{min} = 0.5E_r(\epsilon_c - \epsilon_t) \tag{31}$$

where

$$E_r = \frac{\sigma_m - \sigma_r}{\epsilon_m - \epsilon_r} \tag{32}$$

$$\epsilon_t = \epsilon_m - \frac{\sigma_m}{E_r} \tag{33}$$

and σ_m and ϵ_m are the stress and strain at the unloading point on the compressive monotonic envelope, respectively. If the unloading–reloading cycle is incomplete, the material response will be a straight line with slope E_c, as shown in Figure 4.

The tensile behavior of concrete model takes into the account tension stiffening and the effects of initial cracking. Details of monotonic and cyclic behavior of concrete model under tensile stress are given by Yassin [50].

Since there are different loading/unloading branches in this model, the energy computation needs to be considered separately for each branch. One energy component that remains the same in all loading cases is the elastic strain energy density E_S, that is a function of current stress only:

$$E_S = E_S(\sigma) = \frac{1}{2E_c}\sigma^2 \tag{34}$$

The incremental form of Equation 34 is:

$$dE_S = \frac{1}{E_c}\sigma d\sigma \tag{35}$$

In order to calculate plastic dissipation, a few assumptions are made in order to ensure that the energy behavior of concrete material follows thermodynamics, as illustrated in Figure 5:

- Majority of energy is dissipated during first loading in compression and/or tension (Figures 5(a) and 5(d)).
- Subsequent cycles of loading, on an already damaged concrete, do not dissipate much energy (Figures 5(b) and 5(c)).
- No energy is dissipated during unloading in both compressive and tensile conditions.
- When the material is cyclically loaded under compression, energy dissipation only happens when the stress reaches the upper bound σ_{max}.
- No energy is dissipated during cyclic loading when the material is under tension.

For a single loading step from stress state a to b in each subplot of Figure 5, the energy dissipation is represented by the shaded area.

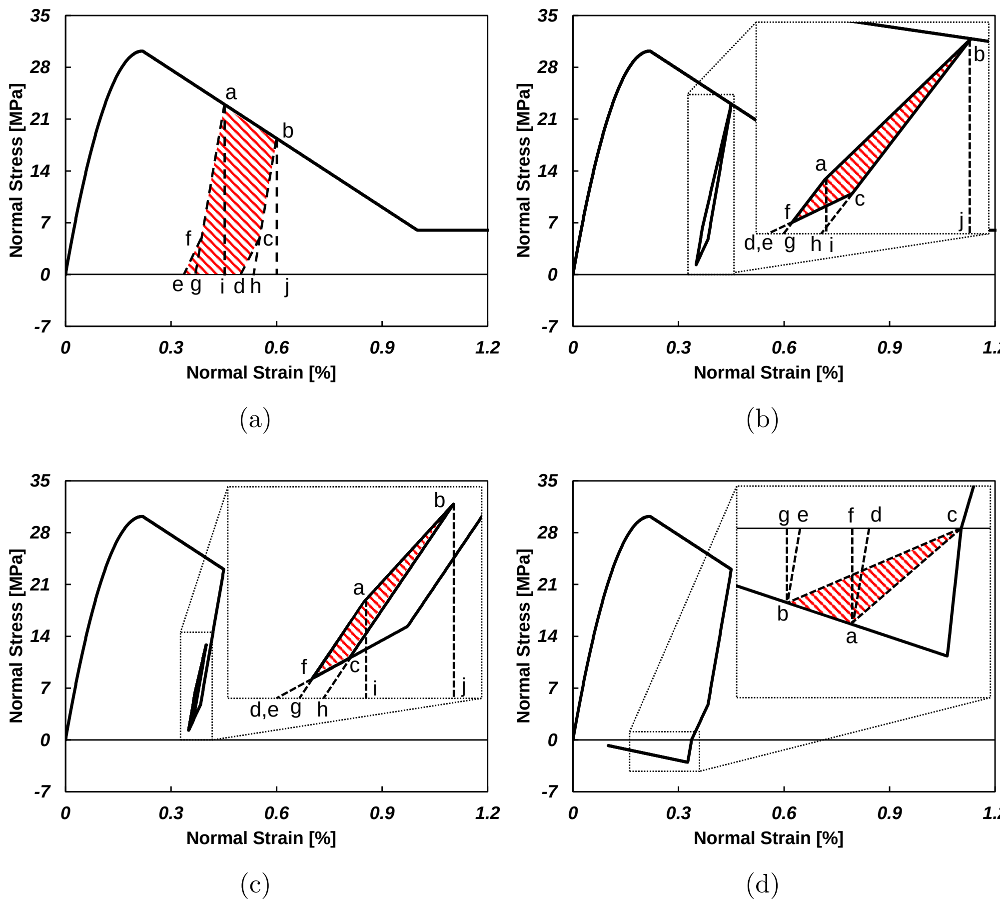

Figure 5: Energy computation of uniaxial concrete fiber: (a) First compression; (b) Single compressive unloading-reloading cycle; (c) Unloading-reloading cycles within compression envelope; (d) First tension.

If the material is under compression (Figures 5(a), 5(b), and 5(c)), the amount of energy dissipated in the concrete fiber D_P is calculated by using the area of a polygon $abcdef$. This polygon is formed by the two unloading paths originating from stress states a and b:

$$dD_P = \frac{1}{2}\left[(\sigma - \sigma_c)d\epsilon + (\epsilon_c - \epsilon)d\sigma + (\epsilon_c - \epsilon_f)\sigma + (\sigma_f - \sigma_c)(\epsilon - \epsilon_t) + \sigma_c d\epsilon_t\right] \tag{36}$$

where the stress and strain at point f can be computed based on equations that define respective unloading paths, using the following expression:

$$\epsilon_f = \frac{\sigma + 0.5E_r\epsilon_t - E_c\epsilon}{0.5E_r - E_c} \qquad \sigma_f = 0.5E_r(\epsilon_f - \epsilon_t) \tag{37}$$

Point c can be calculated using the same approach, by using all stress and strain variables evaluated at state b.

Note that the polygon becomes quadrilateral in the cases of cyclic loading within the monotonic envelope, as can be observed in Figure 5 (b) and (c). Nevertheless, Equations 36 and 37 remain valid.

Plastic free energy E_P of concrete material is calculated by using the triangular area fge at state a:

$$E_P = \frac{1}{2}\left[\left(\epsilon - \frac{\sigma}{E_c} - \epsilon_t\right)\sigma_f\right] \tag{38}$$

The incremental form of Equation 38 is obtained by taking the difference between the plastic free energy at states a and b:

$$dE_P = \frac{1}{2}\left[\left(\sigma_c - \sigma_f - \frac{1}{E_c}\sigma\right)(\epsilon - \epsilon_t) - (d\epsilon - d\epsilon_t)\sigma_c - \frac{1}{E_c}\sigma c d\sigma\right] \tag{39}$$

Adding Equation 35, 36, and 39 yields the incremental form of energy balance:

$$dE_S + dE_P + dD_P = \sigma d\epsilon \tag{40}$$

where the increment of three energy components add up to the increment of stress power during any loading step.

3. Numerical Studies

Numerical examples presented in this paper are all simulated using the MS-ESSI Simulator [17], and are available on the MS-ESSI website http://ms-essi.info/. Energy dissipation is calculated for beam finite elements made up from inelastic concrete and steel fiber sections

We begin by performing numerical simulation of steel and plain concrete columns under various loading conditions. This is done to study the energy behavior of uniaxial steel and concrete material models. Then, a model of reinforced concrete column, consisting of concrete and steel fibers, is constructed and simulated to illustrate the energy dissipation in reinforced concrete structural elements. Finally, a steel frame structure is modeled with fiber section elements and loaded with dynamic, seismic motion. Through these examples, it will be shown that the difference between plastic work and plastic energy dissipation can be significant.

External loads are applied incrementally using displacement-control scheme. System of equations are solved using Newton-Raphson equilibrium iteration algorithm [7] and UMFPACK solver [9], within MS-ESSI Simulator [17]. Static, displacement control, integration algorithm is used for the column loading cases, while Newmark integration is used for the dynamic steel frame case. Note that viscous and numerical damping are excluded from all cases, in order to accurately evaluate energy dissipation due to material elastoplasticity. In other words, no viscous damping (Rayleigh or Caughey) is used, and for Newmark time integration algorithm [31], $\beta = 0.25$ and $\gamma = 0.5$ parameters are used.

3.1. Steel Column

In order to verify the proposed energy computation approach for uniaxial steel material model, examples of steel columns are studied in this section. As shown in Figure 6, the one meter long column model is fixed at the bottom, and loads are applied at the top. The size of the cross section is

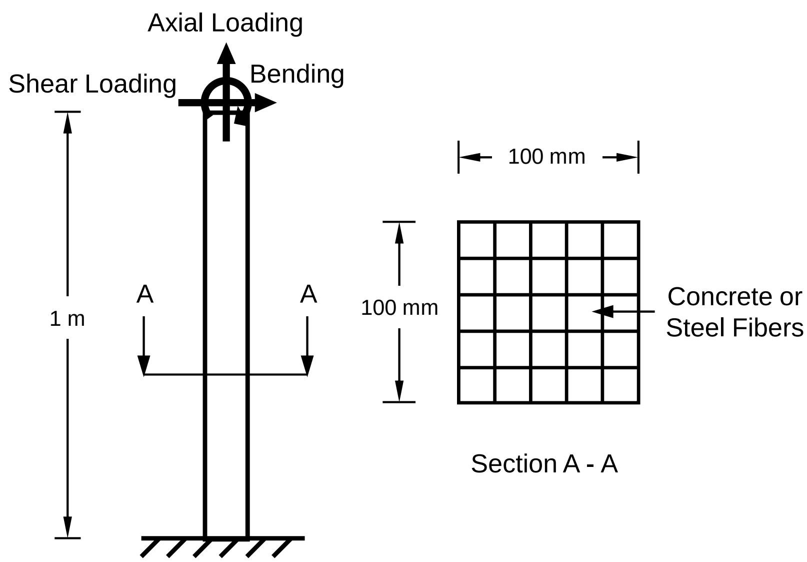

Figure 6: Schematic of the steel/plain-concrete column modeled with fiber sections and uniaxial steel/concrete materials.

100mm × 100mm. The parameters for uniaxial steel material used in this section are summarized in Table 1. Material model used for steel is based on Menegotto and Pinto [27] and Filippou et al. [14], as noted in section 2.1.

Table 1: Material model parameters used in steel column examples.

σ_y [MPa]	E [GPa]	b	R_0	c_{R_1}	c_{R_2}	a_1	a_2	a_3	a_4
413.8	200.0	0.01	18.0	0.925	0.15	0.0	55.0	0.0	55.0

3.1.1. Cyclic Axial Loading

The evolution of energy parameters for uniaxial steel material are computed using Equations 19, 20, and 22. Figure 7 shows the stress–strain response as well as the energy calculation results of the steel column under cyclic axial loading.

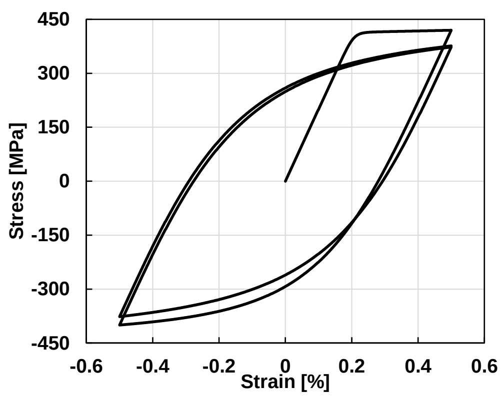

(a)

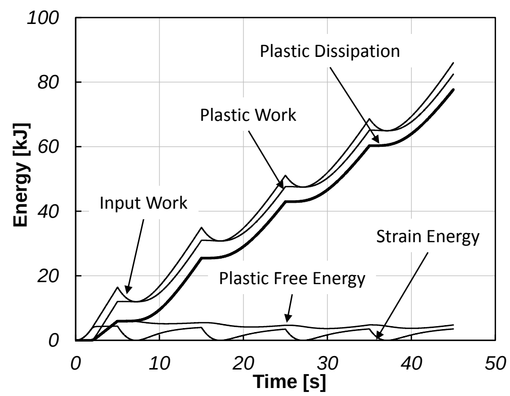

(b)

Figure 7: Energy analysis of steel column under cyclic axial loading: (a) Cyclic stress–strain response; (b) Evolution of different forms of energy with cycles: Input work, plastic dissipation, plastic work, plastic free energy, and strain energy.

As expected, the stress–strain response shown in Figure 7 follows the constitutive model presented in Figure 2. Due to the choice of hardening parameters (a_1, a_2, a_3, and a_4), isotropic hardening after first loading reversal is relatively small. The evolution of plastic free energy, which is related to the hardening behavior of the constitutive model, is also observed to be insignificant after the first loading reversal. Energy balance in the steel material (Equation 23) is maintained during entire simulation.

In this particular case, the difference between plastic dissipation and plastic work is significant during initial loading (or monotonic loading), but then becomes less significant during cyclic loading. It is important to point out that such difference could be significant if different hardening parameters are chosen or complex loading conditions (for example seismic loading) are applied.

Another observation is that the ratio between plastic dissipation and plastic work, the Quinney–Taylor coefficient [44], changes from 0.5 to 0.9 in just a few loading cycles. Based on this, it is recommended that Quinney–Taylor coefficient be variable, calculated directly, as was done here, and not prescribed as a fixed number.

3.1.2. Cyclic Bending Loading

The same column used in section 3.1 is loaded with cyclic bending moment on the top. Figure 8 shows the moment–rotation response as well as the energy calculation results for the steel column under cyclic bending loading.

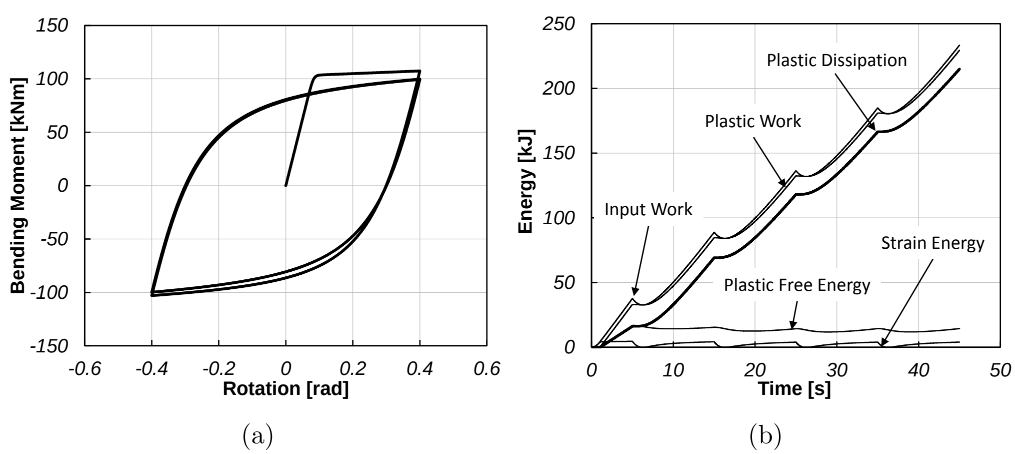

Figure 8: Energy analysis of steel column under cyclic bending loading: (a) Moment–rotation response; (b) Evolution of different forms of energy with cycles: Input work, plastic dissipation, plastic work, plastic free energy, and strain energy.

When a beam element is loaded in pure bending, half of the fibers will be in tension while the other half in compression. The normal stress and strain distribution on any cross section is symmetric. Since the fiber material model used in this case has the same stress–strain response under tension and compression, the energy results in for this bending case share the similar pattern with those in the axial loading case.

Note that in both axial and bending cases, the strain energy accumulated in the material body is much smaller than the plastic dissipation. This means that most of the input work results in plastic deformation of the material, and indicates possibility of large deformation and material damage.

3.2. Plain Concrete Column

In order to verify the proposed energy computation approach for uniaxial concrete material model, examples of plain concrete columns are studied in this section. The size and setup of the model are the same as those of the steel column, which has been shown in Figure 6. The parameters for uniaxial concrete material used in this section are summarized in Table 2.

Table 2: Material model parameters used in plain concrete column examples.

f_{cs} [MPa]	ϵ_{cs}	f_{cu} [MPa]	ϵ_{cu}	λ	f_{ts} [MPa]	E_t [GPa]
-30.2	-0.00219	-6.0	-0.00696	0.5	3.02	5.0

3.2.1. Monotonic Axial Loading

As stated in the assumptions for energy dissipation in the uniaxial concrete model, the amount of energy dissipated during monotonic loading is much larger than that during subsequent unloading/reloading. Such assumption is made based on the brittle nature of concrete materials, in which damage caused by fracture is the main source of energy dissipation. In this case, the stress–strain response as well as the energy results of the plain concrete column model under monotonic axial compression is investigated and presented in Figure 9.

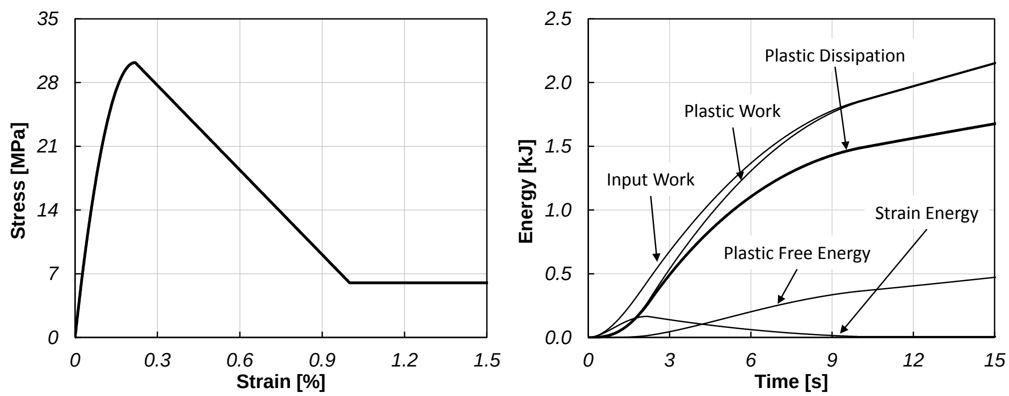

(a) (b)

Figure 9: Energy analysis of plain concrete column under monotonic axial loading: (a) Stress–strain response; (b) Evolution of different forms of energy with cycles: Input work, plastic dissipation, plastic work, plastic free energy, and strain energy.

The stress–strain response shown in Figure 9 follows the compressive constitutive response as presented in Figure 4. Energy balance of the model, expressed by Equation 40, is maintained during entire simulation.

As observed in Figure 9, large amount of the input work is dissipated during monotonic compression. It is important to point out that the difference between plastic dissipation and plastic work is significant. Plastic free energy starts to accumulate after maximum compressive strength is reached and continue to increase even after crushing. Such behavior can be explained by considering that the micro-structure of concrete continues to evolve as external loads continues to be applied on the solid/structure.

The strain energy starts to decrease after maximum compressive strength is reached and gradually decreases to almost zero after crushing. This observation is consistent with the fact that the micro-fractures expand rapidly after maximum strength is reached, which leads to the release of elastic strain energy and energy dissipation caused by fracture and crushing.

3.2.2. Cyclic Axial Loading

Due to the complex unloading–reloading rules of the model, the cyclic behavior of the uniaxial concrete material is much more complicated than that of the steel model. Figure 10 presents the stress–strain response as well as the energy calculation results for the plain concrete column under cyclic axial loading.

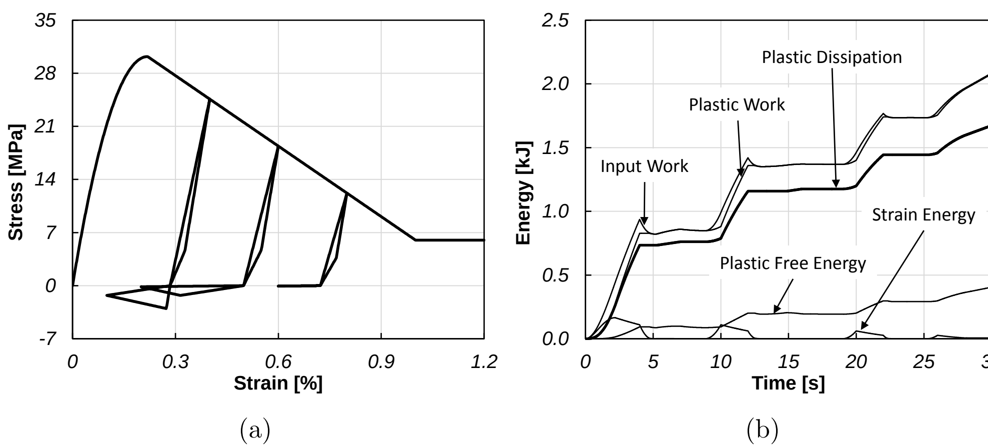

Figure 10: Energy analysis of plain concrete column under cyclic axial loading: (a) Stress–strain response; (b) Evolution of different forms of energy with cycles: Input work, plastic dissipation, plastic work, plastic free energy, and strain energy.

As shown in Figure 10, the majority of plastic dissipation occurs during initial, monotonic loading branch. It is important to note that there are negative increments in plastic work during unloading, for example at time $t = 5\text{s}$, however plastic dissipation never shows any negative increments.

This is consistent with the requirements of the second law of thermodynamics (Equation 11).

It should be mentioned that there is a small amount of energy dissipation when the material is in tension, for example between $t = 6 - 9$s. However, this energy dissipation is much smaller than that when the material is in compression. This can be explained by the low tensile strength of concrete material in general.

3.3. Reinforced Concrete Column

To study the combined influence of concrete and steel fibers, energy calculations for a reinforced concrete column are presented. The schematic of the model is shown in Figure 10, and the material model parameters are summarized in Table 3. The cross section of the column is modeled with unconfined concrete, confined concrete, and steel fibers with uniaxial material models discussed in earlier sections.

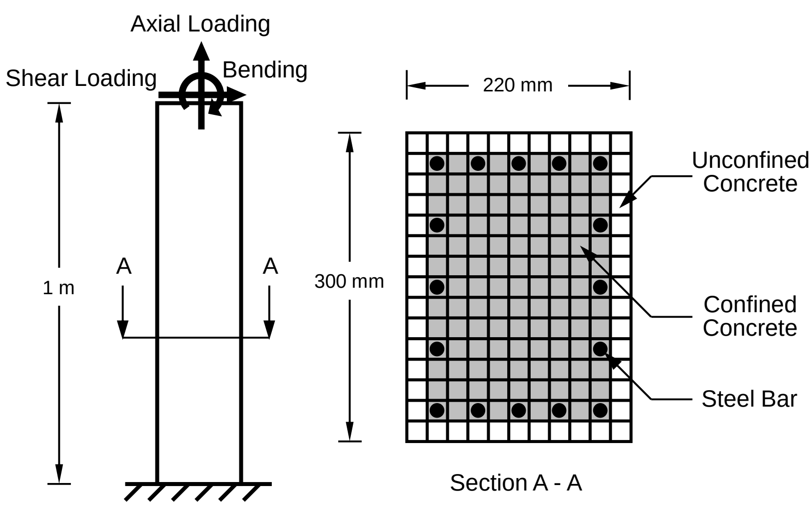

Figure 11: Schematic of the reinforced concrete column modeled with fiber sections and uniaxial steel/concrete materials.

Table 3: Material model parameters used in reinforced concrete column examples.

Steel Fiber		Concrete Fiber		
			Confined	**Unconfined**
σ_y (MPa)	413.8	f_{cs} (MPa)	-30.2	-24.16
E (GPa)	200.0	ϵ_{cs}	-0.00219	-0.001752
b	0.01	f_{cu} (MPa)	-6.0	0.0
R_0	18.0	ϵ_{cu}	-0.00696	-0.005568
c_{R_1}	0.925	λ	0.5	0.5
c_{R_2}	0.15	f_{ts} (MPa)	3.02	0.0
a_1, a_3	0.0	E_t (GPa)	5.0	0.0
a_2, a_4	55.0			

3.3.1. Cyclic Axial Loading

Figure 12 shows the force–displacement response as well as the energy calculation results for the reinforced concrete column under cyclic axial loading.

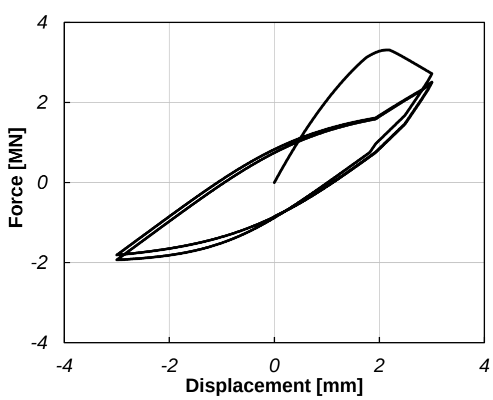

(a)

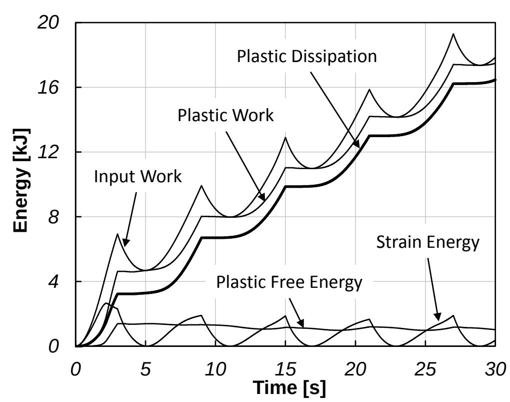

(b)

Figure 12: Energy analysis of reinforced concrete column under cyclic axial loading: (a) Force–displacement response; (b) Evolution of different forms of energy with cycles: Input work, plastic dissipation, plastic work, plastic free energy, and strain energy.

Since concrete fibers have much higher compressive strength than tensile strength, the stress–strain response of the column is controlled by the concrete part when it is under compression, and by the steel part when under tension. In this case, the initial loading curve clearly resembles the stress–strain response of concrete fiber under monotonic compression. Then the unloading–reloading cycles have the same pattern as those of the steel fiber under cyclic axial loading.

By comparing the energy results for reinforced concrete shown in Figure 12 and those for steel shown in Figure 7, it can be seen that the energy dissipation patterns in both cases are similar after initial compression and tension of concrete, after which steel takes over. This indicates that the majority of input work is dissipated in the steel fibers once the maximum strength of the concrete is exceeded. Again, it can be observed that the difference between plastic work and plastic dissipation is significant in this case.

3.3.2. Cyclic Bending Loading

Figure 13 shows the moment–rotation response as well as the energy calculation results of the reinforced concrete column under cyclic pure bending loading.

During initial loading, the concrete fibers on the compressive side of the cross section take most of the compression, while during the first reverse loading, the concrete fibers on the other side of the cross section are compressed and damaged. This process is indicated in the moment–rotation curve where two bumps, for positive and negative moments, are observed. The energy computation results also show that the concrete fibers dissipate large amount of energy and get damaged during the first loading cycle. After

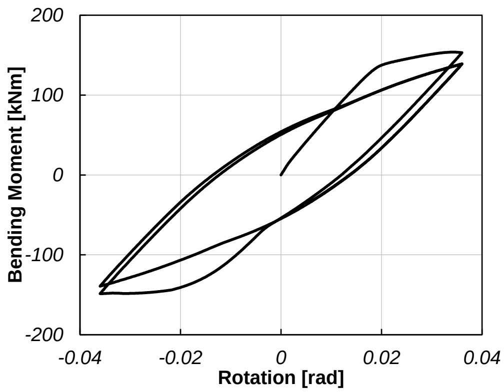

(a)

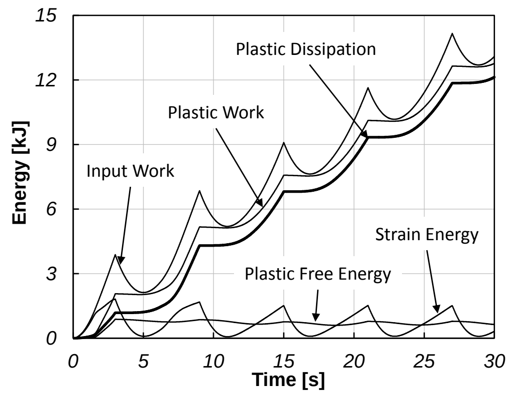

(b)

Figure 13: Energy analysis of reinforced concrete column under cyclic bending loading: (a) Moment–rotation response; (b) Evolution of different forms of energy with cycles: Input work, plastic dissipation, plastic work, plastic free energy, and strain energy.

that, the response of the reinforced concrete column is controlled by the steel bars.

According to the two cases, axial and pure bending, of reinforced concrete column under cyclic loading, the concrete part of the column can dissipate the majority of the input work if the loading is mainly monotonic compression. For cyclic loading cases, if the loading does not exceed the maximum compressive strength of the concrete, energy dissipation is observed in both the concrete and steel. However, if the cyclic loading does exceed the maximum strength of the concrete, the majority of energy dissipation is in the steel reinforcing bars after the concrete is damaged. This conclusion is consistent with the engineering experience that reinforcement is crucial to the performance of concrete structure during seismic events, when the beams and columns suffer from cyclic loadings.

3.4. Steel Frame

Previous examples were assumed to be static or quasi-static, cyclic. This was done in order investigate the energy dissipation on material and simple structure level without the influence of dynamics. In other words, kinetic energy was not considered. This example features a full dynamic modeling of a steel frame using fiber section elements with uniaxial steel material, as shown in Figure 14. Model is comprised of three levels, floors. Each level of this frame is comprised of two vertical columns (beam-column elements) and one horizontal beam (beam-column element) on top of these columns. Steel frame model is loaded dynamically at the base using 1D seismic motion. The peak acceleration of the input motion is 0.76 g.

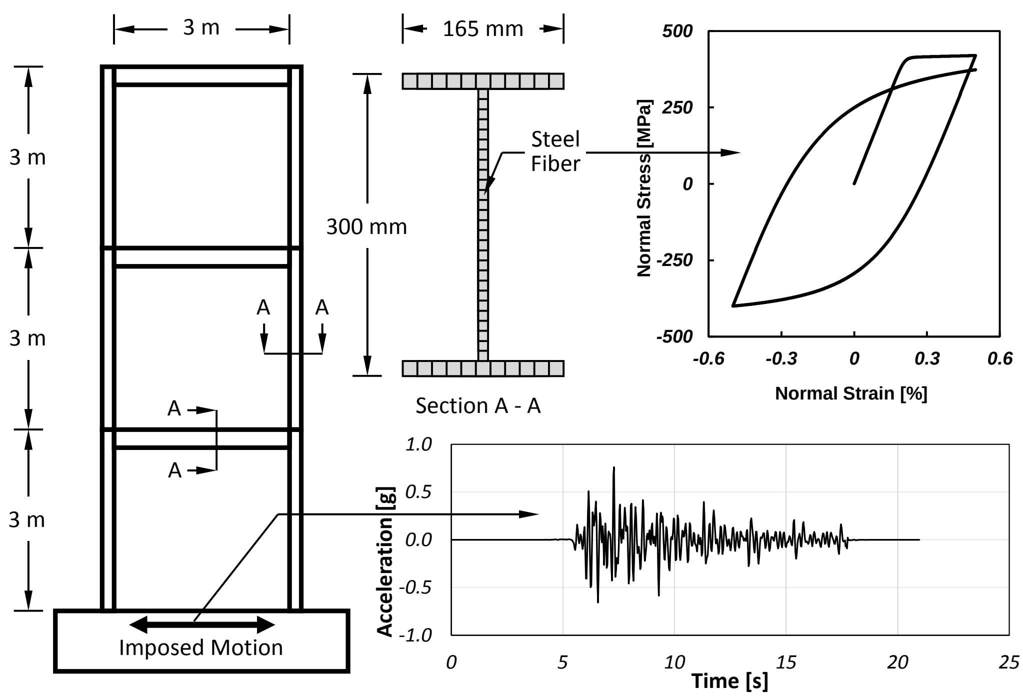

Figure 14: Schematic of the steel frame modeled with fiber section elements and uniaxial steel material.

The energy computation results are shown in Figure 15. Input work is computed from the input motion and reaction forces at the base of model. Kinetic energy is computed from velocities of nodes. Strain energy, plastic free energy, and plastic dissipation at each level are computed using Equation 19, 20, and 22.

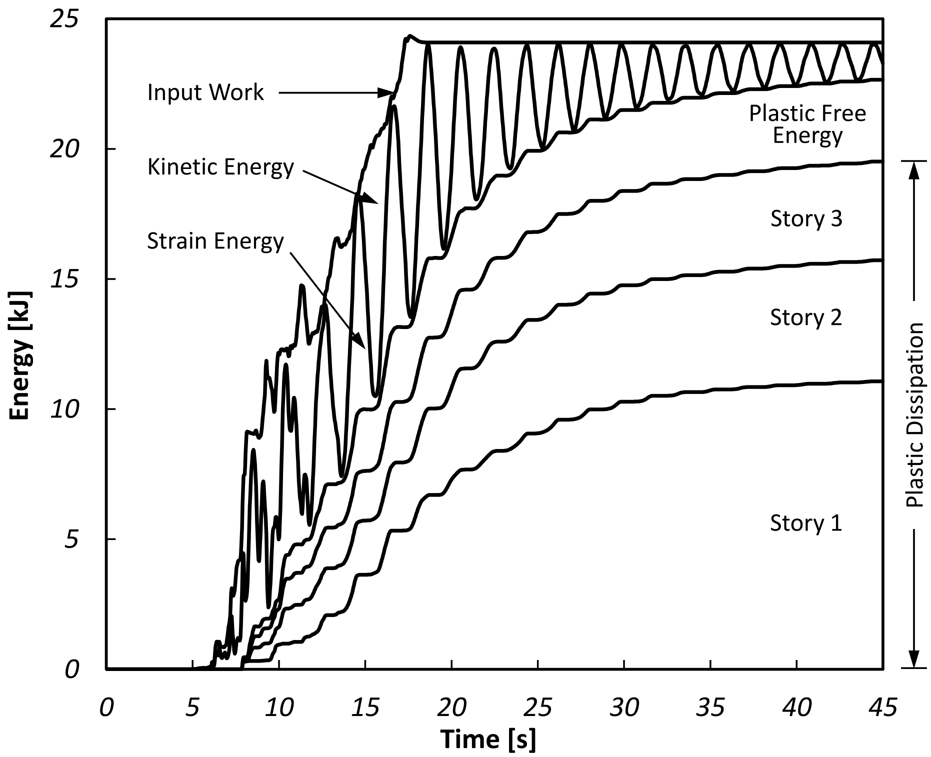

Figure 15: Energy analysis of steel frame model under imposed seismic motion.

It is noted that the energy balance if fully maintained at all times. It is observed in Figure 15, that the sum of kinetic energy, strain energy, plastic free energy, and plastic dissipation of the system equals to the total input work. All of the above energies are calculated independently, and then used to prove energy balance of the system.

Close inspection of curve above plastic free energy (curve that represents sum of plastic dissipation for all three levels, and plastic free energy, reveals small negative slope. This curve represents plastic work and not plastic dissipation hence negative slope is allowed. On the other hand, curve representing sum of plastic dissipation for all three levels, does not, and cannot have negative slope. Negative slope of this plastic dissipation curve would mean energy production and that would violate second law of thermodynamics [49]. At the end of simulation, more than 80% of the total input work is dissipated due to material elasto-plasticity. Approximately 13% of input work is transformed into plastic free energy that does not result in heating or material damage.

4. Conclusions

Presented in this paper was a thermodynamic-based methodology for computation of energy dissipation in nonlinear structural elements, modeled using fiber section and uniaxial material models. Two popular material models for steel and concrete were examined, with focus on their nonlinear cyclic behaviors. Formulation for the energy storage and dissipation in these two material models were derived from the basic principles of thermodynamics, in combination with a few reasonable assumptions. The proposed methodology was illustrated using a series of numerical simulations on beam column finite elements subjected to axial and bending loads. In addition, energy calculations were performed for a three story steel frame, excited with a 1D seismic motion at the base.

The misconception about plastic work and plastic dissipation, which leads to the violation of principles of thermodynamics, and that is found in a number of papers on energy dissipation of structures, was addressed. Theoretical derivation and experimental observation have both proven that plastic free energy is a basic form of energy that should not be neglected. Taking into account kinetic energy, strain energy, plastic free energy, and plastic dissipation, ensures that the first law of thermodynamics, energy balance, is maintained.

Based on experimentally observed behavior of concrete and steel, few assumptions were made within concrete and steel 1D fiber material models to enforce thermomechanics. Equations for energy computation were derived and implemented in MS-ESSI [17]. In addition, numerical examples presented in this paper are available on the MS-ESSI website http://ms-essi.info/.

Presented approach was illustrated and tested using several concrete, steel and reinforced concrete beam-column element and a steel frame with different loading conditions. As expected, energy balance was maintained during entire simulation in all tested cases. It was shown that plastic work could drop, have negative increments, however plastic dissipation was always non negative, as expressed by the second law of thermodynamics. It was also observed that the difference between plastic work and plastic dissipation could be significant. The ratio between plastic work and plastic dissipation, Quinney–Taylor coefficient, did evolve in time. It is thus recommended not to use a constant value for Quinney–Taylor coefficient, rather it should be calculated on a case by case basis.

5. Acknowledgments

This work was supported in part by the US-DOE.

References

[1] T. Belytschko, B. Moran, and M. Kulkarni. On the crucial role of imperfections in quasi-static viscoplastic solutions. *Journal of Applied Mechanics*, 58:658–665, 1991.

[2] J. F. Besseling and E. Van Der Giessen. *Mathematical modeling of inelastic deformation*, volume 5. CRC Press, 1994.

[3] G. Chang and J. B. Mander. *Seismic energy based fatigue damage analysis of bridge columns: Part I-Evaluation of seismic capacity.* National Center for Earthquake Engineering Research Buffalo, NY, 1994.

[4] I. Collins. Associated and non-associated aspects of the constitutive laws for coupled elastic/plastic materials. *International Journal of Geomechanics*, 2(2):259–267, 2002.

[5] I. Collins and P. Kelly. A thermomechanical analysis of a family of soil models. *Geotechnique*, 52(7):507–518, 2002.

[6] I. F. Collins and G. T. Houlsby. Application of thermomechanical principles to the modelling of geotechnical materials. *Procedings of Royal Society London*, 453:1975–2001, 1997.

[7] M. A. Crisfield. Consistent schemes for plasticity computation with the Newton Raphson method. *Computational Plasticity Models, Software, and Applications*, 1:136–160, 1987.

[8] Y. Dafalias, D. Schick, C. Tsakmakis, K. Hutter, and H. Baaser. A simple model for describing yield surface evolution. In *Lecture note in applied and computational mechanics*, pages 169–201. Springer, 2002.

[9] T. Davis. Algorithm 832: Umfpack, an unsymmetric-pattern multifrontal method. *ACM Transactions on Mathematical Software*, 30(2): 196–199, 2004. URL http://doi.acm.org/10.1145/992200.992206.

[10] D. Deniz, J. Song, and J. F. Hajjar. Energy-based seismic collapse criterion for ductile planar structural frames. *Engineering Structures*, 141:1–13, 2017.

[11] M. Dolinski, D. Rittel, and A. Dorogoy. Modeling adiabatic shear failure from energy considerations. *Journal of the Mechanics and Physics of Solids*, 58(11):1759–1775, 2010.

[12] W. Farren and G. Taylor. The heat developed during plastic extension of metals. *Proceedings of the royal society of London A: mathematical, physical and engineering sciences*, 107(743):422–451, 1925.

[13] H. P. Feigenbaum and Y. F. Dafalias. Directional distortional hardening in metal plasticity within thermodynamics. *International Journal of Solids and Structures*, 44(22-23):7526–7542, 2007.

[14] F. C. Filippou, V. V. Bertero, and E. P. Popov. Effects of bond deterioration on hysteretic behavior of reinforced concrete joints. Technical report, Earthquake Engineering Research Center, University of California, Berkeley, 1983.

[15] S. Gajan and D. S. Saravanathiiban. Modeling of energy dissipation in structural devices and foundation soil during seismic loading. *Soil Dynamics and Earthquake Engineering*, 31(8):1106 – 1122, 2011. ISSN 0267-7261. doi: 10.1016/j.soildyn.2011.02.006. URL http://www.sciencedirect.com/science/article/pii/S0267726111000923.

[16] J. Hodowany, G. Ravichandran, A. Rosakis, and P. Rosakis. Partition of plastic work into heat and stored energy in metals. *Experimental mechanics*, 40(2):113–123, 2000.

[17] B. Jeremić, G. Jie, Z. Cheng, N. Tafazzoli, P. Tasiopoulou, F. P. J. A. Abell, K. Watanabe, Y. Feng, S. K. Sinha, F. Behbehani, H. Yang, and H. Wang. *The MS ESSI / Real ESSI Simulator System*. University of California, Davis and Lawrence Berkeley National Laboratory, 2018. http://ms-essi.info/.

[18] E. Kalkan and S. Kunnath. Effective cyclic energy as a measure of seismic demand. *Journal of Earthquake Engineering*, 11(5):725–751, 2007.

[19] D. Kent and R. Park. Flexural members with confined concrete. *ASCE Journal of Structural Division*, 97:1969–1990, 1971.

[20] K. Kolozvari, K. Orakcal, and J. Wallace. Shear-flexure interaction modeling for reinforced concrete structural walls and columns under reversed cyclic loading. Technical Report PEER Report No. 2015/12, Pacific Earthquake Engineering Research Center, Pacific Earthquake Engineering Research Center, Richmod, CA, December 2015.

[21] W.-P. Kwan and S. Billington. Simulation of structural concrete under cyclic load. *Journal of Structural Engineering*, 127(12):1391–1401, 2001.

[22] J. Lee and G. L. Fenves. Plastic-damage model for cyclic loading of concrete structures. *Journal of engineering mechanics*, 124(8):892–900, 1998.

[23] P. Léger and S. Dussault. Seismic-energy dissipation in mdof structures. *Journal of Structural Engineering*, 118(5):1251–1269, 1992.

[24] J. Lubliner. On the thermodynamic foundations of non-linear solid mechanics. *International Journal of Non-Linear Mechanics*, 7:237–254, 1972.

[25] J. B. Mander, M. J. Priestley, and R. Park. Theoretical stress-strain model for confined concrete. *Journal of structural engineering*, 114(8): 1804–1826, 1988.

[26] J. Mason, A. Rosakis, and G. Ravichandran. On the strain and strain rate dependence of the fraction of plastic work converted to heat: an experimental study using high speed infrared detectors and the kolsky bar. *Mechanics of Materials*, 17(2-3):135–145, 1994.

[27] M. Menegotto and P. E. Pinto. Method of analysis for cyclically loaded reinforced clncrete plane frames including changes in geometry and non-elastic behaviour of elements under combined normal force and bending. In *Proceedings of IABSE Symposium*, pages 15–22, 1973.

[28] M. G. Mezgebo and E. M. Lui. A new methodology for energy-based seismic design of steel moment frames. *Earthquake Engineering and Engineering Vibration*, 16(1):131–152, 2017.

[29] A. Moustafa. Damage-based design earthquake loads for single-degree-of-freedom inelastic structures. *Journal of structural engineering*, 137 (3):456–467, 2011.

[30] M. Nehdi, M. S. Alam, and M. Youssef. Development of corrosion-free concrete beam–column joint with adequate seismic energy dissipation. *Engineering Structures*, 32(9):2518–2528, 2010.

[31] N. M. Newmark. A method of computation for structural dynamics. *ASCE Journal of the Engineering Mechanics Division*, 85:67–94, July 1959.

[32] E. Nikbakht, K. Rashid, F. Hejazi, and S. A. Osman. A numerical study on seismic response of self-centring precast segmental columns at different post-tensioning forces. *Latin American Journal of solids and structures*, 11(5):864–883, 2014.

[33] S. Osovski, D. Rittel, and A. Venkert. The respective influence of microstructural and thermal softening on adiabatic shear localization. *Mechanics of Materials*, 56:11–22, 2013.

[34] S. Popovics. A numerical approach to the complete stress-strain curve of concrete. *Cement and concrete research*, 3(5):583–599, 1973.

[35] G. Ravichandran, A. J. Rosakis, J. Hodowany, P. Rosakis, M. D. Furnish, N. N. Thadhani, and Y. Horie. On the conversion of plastic work into heat during high-strain-rate deformation. In *AIP conference proceedings*, volume 620/1, pages 557–562. AIP, 2002.

[36] P. Rosakis, A. Rosakis, G. Ravichandran, and J. Hodowany. A thermodynamic internal variable model for the partition of plastic work into heat and stored energy in metals. *Journal of the Mechanics and Physics of Solids*, 48(3):581–607, 2000.

[37] B. Scott, R. Park, and M. Priestley. Fiber element modeling for seismic performance of bridge columns made of concrete-filled frp tubes. *Journal of the American Concrete Institute*, 79(1):13–27, 1982.

[38] S. J. Semnani, J. A. White, and R. I. Borja. Thermoplasticity and strain localization in transversely isotropic materials based on anisotropic critical state plasticity. *International Journal for Numerical and Analytical Methods in Geomechanics*, 40(18):2423–2449, 2016.

[39] T. Soong and B. Spencer. Supplemental energy dissipation: state-of-the-art and state-of-the-practice. *Engineering Structures*, 24(3):243–259, 2002.

[40] E. Spacone, F. C. Filippou, and F. F. Taucer. Fibre beam-column model for non-linear analysis of r/c frames: Part i. formulation. *Earthquake Engineering & Structural Dynamics*, 25(7):711–725, July 1996.

[41] E. Spacone, F. C. Filippou, and F. F. Taucer. Fibre beam-column model for non-linear analysis of r/c frames: Part ii. applicationss. *Earthquake Engineering & Structural Dynamics*, 25(7):727–742, July 1996.

[42] M. Symans and M. Constantinou. Passive fluid viscous damping systems for seismic energy dissipation. *ISET Journal of Earthquake Technology*, 35(4):185–206, 1998.

[43] M. Symans, F. Charney, A. Whittaker, M. Constantinou, C. Kircher, M. Johnson, and R. McNamara. Energy dissipation systems for seismic applications: current practice and recent developments. *Journal of structural engineering*, 134(1):3–21, 2008.

[44] G. I. Taylor and H. Quinney. The latent energy remaining in a metal after cold working. *Proceedings of the Royal Society of London. Series A, Containing Papers of a Mathematical and Physical Character*, 143 (849):307–326, 1934.

[45] C.-M. Uang and V. V. Bertero. Evaluation of seismic energy in structures. *Earthquake Engineering & Structural Dynamics*, 19(1):77–90, 1990.

[46] Y. Wang, Z. Y. Bu, and L. Hu. Seismic behavior of precast segmental bridge columns with carbon fibre reinforcement as energy dissipation bars. In *Applied Mechanics and Materials*, volume 157, pages 1148–1152. Trans Tech Publ, 2012.

[47] J. D. Waugh. *Nonlinear analysis of T-shaped concrete walls subjected to multi-directional displacements*. Iowa State University, 2009.

[48] K. Wong. Seismic energy dissipation of inelastic structures with tuned mass dampers. *Journal of engineering mechanics*, 134(2):163–172, 2008.

[49] H. Yang, S. K. Sinha, Y. Feng, D. B. McCallen, and B. Jeremić. Energy dissipation analysis of elastic-plastic materials. *Computer Methods in Applied Mechanics and Engineering*, 331:309–326, 2017.

[50] M. H. M. Yassin. *Nonlinear analysis of prestressed concrete sructures under monotonic and cyclic loads*. PhD thesis, University of California, Berkeley, 1994.

[51] Y.-y. Zhang, K. A. Harries, and W.-c. Yuan. Experimental and numerical investigation of the seismic performance of hollow rectangular bridge piers constructed with and without steel fiber reinforced concrete. *Engineering Structures*, 48:255–265, 2013.

[52] M. Zhou, G. Ravichandran, and A. Rosakis. Dynamically propagating shear bands in impact-loaded prenotched platesii. numerical simulations. *Journal of the Mechanics and Physics of Solids*, 44(6):1007–1032, 1996.

[53] Z. Zhu, I. Ahmad, and A. Mirmiran. Fiber element modeling for seismic performance of bridge columns made of concrete-filled frp tubes. *Engineering structures*, 28(14):2023–2035, 2006.